PREDIS

Deliverable 6.7
Modelling tool to predict behaviour of reconditioned wastes

28.08.2024 Version Final

Dissemination level: Public

Suresh Seetharam

Belgian Nuclear Research Centre
Waste and Disposal Expert Group
Boeretang 200, Mol-2400
Belgium

suresh.seetharam@sckcen.be

This project has received funding from the Euratom research and training programme 2019-2020 under grant agreement No 945098.

Project acronym PREDIS	Project title PRE-DISposal management of radioactive waste		Grant agreement No. 945098
Deliverable No. D7.5	Deliverable title Modelling tool to predict behaviour of reconditioned wastes		Version Final
Type Report	Dissemination level Public		Due date M48
Lead beneficiary SCK CEN			WP No. 6
Main author Suresh Seetharam (SCK CEN)	Reviewed by Thierry Mennecart (SCK CEN), WP6 Leader	Accepted by Maria Oksa (VTT), Coordinator	
Contributing authors Vojtěch Galek (CVRez), Quoc Tri Phung (SCK CEN), Anna Sears (CVRez), Lander Frederickx (SCK CEN), Eduardo Ferreira (SCK CEN)			Pages 27

Abstract

Some radioactively contaminated solid organic waste streams are problematic to dispose of by direct immobilization in traditional cementitious binders, as they can potentially degrade after disposal, possibly resulting in the release of radionuclides. Therefore, within Work Package 6 of the PREDIS project, alternative technologies for the treatment and disposal of these waste streams were investigated. In particular, alkali-activated material (AAM) and a blended cementitious matrix were examined, which ensured good mechanical properties while exhibiting good long-term durability. The focus of the study presented in this report is on the thermal evolution of the reconditioned waste at the drum scale. For traditional cementitious binders, the absolute value of the peak temperature that develops in a waste drum is an important consideration for minimizing pathologies related to delayed ettringite formation or cracking owing to thermal stresses. However, for the binders pursued in WP6, such prescriptions do not exist because similar pathologies have not yet been reported. Nevertheless, it is worthwhile to gain an understanding of maximum temperatures that potentially develop at the drum scale with these modern binders so that additional studies can be set up to understand the impact of high temperature on the material integrity.

This report presents an experimental-numerical study of the thermal evolution of reconditioned MSO residue waste emplaced in 100 L drums. Three binders, viz., (i) AAM with metakaolin precursor (AAM_MK), (ii) AAM with BFS precursor, and (iii) blended cement mix with supplementary cementitious material, were used for this purpose with various waste loadings. The study mainly considered isothermal calorimetry experiments of all the above recipes at the SCK CEN to develop a comprehensive dataset of hydration curves that form a direct input to a heat transfer model. Drum-scale experiments on reconditioned MSO residue waste were successfully designed and executed by CVRez. The thermal evolution in the drum was captured using thermal sensors placed at various locations. A standard heat transfer model was used for blind predictions of thermal evolution in the drum. As the drum-scale experiments were conducted only with the AAM_MK binder with 15% waste loading, the drum scale thermal evolution of the remaining recipes was purely a theoretical estimate based on the numerical model.

The calorimetric measurements of the different waste forms showed that the addition of molten salt residue delayed hydration/geopolymerization in both cementitious and alkali-activated matrices. The numerical model captured the main features of the thermal evolution, particularly the peak measured temperature data (> 90 °C) at the core of the AAM_MK binder. It is therefore anticipated that for typical drum sizes (> 200 L) used in pre-disposal storage, the peak temperatures could far exceed 100 °C. Thus, this may warrant further studies on the long-term stability of reconditioned waste forms exposed to high early age temperatures.

This report is a result of the collaboration between SCK CEN and CVReZ.

Keywords

Thermal simulations, Reconditioned waste, Calorimetry, Solid organic waste, Drum scale

Coordinator contact
Maria Oksa
VTT Technical Research Centre of Finland Ltd
Kivimiehentie 3, Espoo / P.O. Box 1000, 02044 VTT, Finland
E-mail: maria.oksa.@vtt.fi
Tel: +358 50 5365 844

Acknowledgement
This project has received funding from the Euratom research and training programme 2019-2020 under grant agreement No 945098.

TABLE OF CONTENTS

1 Introduction

Some radioactively contaminated solid organic waste streams are problematic to dispose of by direct immobilization in traditional cementitious binders, as they can potentially degrade after disposal, possibly resulting in the release of radionuclides. Therefore, within Work Package 6 of the PREDIS project, alternative technologies for the treatment and disposal of these waste streams were investigated [1]. One of the possible ways of treatment is the molten salt oxidation (MSO) process, in which the bulk of organic waste can be oxidized at a high temperature in the presence of a sodium carbonate salt [1][2]. The residue after the MSO process was a salt-containing radionuclide in carbonate form. Separate studies have been conducted to investigate the immobilization technology for this salt residue in an alkali-activated or blended cementitious matrix that ensures good mechanical properties while exhibiting good long-term durability. The focus of the study presented in this report is on the thermal behaviour of the reconditioned waste at the drum scale.

For traditional cementitious binders, the absolute value of the peak temperature that develops in a waste drum is an important consideration for minimizing pathologies related to delayed ettringite formation or cracking due to thermal stresses. Typically, a preventative prescription is to minimize the peak temperature to below 60 °C in the waste drums. However, for the binders pursued in this WP6, such prescriptions do not exist because similar pathologies have not yet been reported. Nevertheless, it is worthwhile to gain an understanding of the maximum temperatures that potentially develop at the drum scale with these modern binders so that additional studies can be conducted to understand the impact of high temperature on material integrity.

Importantly, drum-scale experiments are resource intensive, and it is not practical to set up as many drum-scale experiments as the number of trial recipes considered in the WP6 study. Therefore, recourse to numerical simulations is invaluable not only from a cost perspective, but also for gaining phenomenological understanding at a larger scale based on a few laboratory-based tests. The goal of this study was to explore the thermal behaviour of three recipes: (i) alkali-activated material with metakaolin (AAM_MK) as the precursor (CVRez), (ii) alkali-activated material with blast furnace slag (BFS) as the precursor (AAM_BFS) (SCK CEN), and (iii) blended cementitious material (SCK CEN). To gain confidence in the numerical heat transport model, a drum scale experiment on a promising recipe, AAM_MK, with 15% waste loading (WL) was carried out by CVRez. In the next step, blind predictions with recipes AAM_BFS and the blended cementitious system were carried out for the same drum scale geometry, and comparisons were made.

The heat transport model requires material parameters such as specific heat capacity, thermal conductivity, bulk density, and, importantly, hydration model parameters. As such, a comprehensive parameter estimation is beyond the scope of this project; therefore, certain assumptions have been made with respect to the specific heat capacity (for some recipes) and thermal conductivity. However, significant efforts have been made to identify hydration model parameters for various recipes, including different levels of waste loading. In particular, where possible, isothermal calorimetry and semi-adiabatic calorimetry tests have been carried out at various temperatures to estimate hydration model parameters. The drum-scale thermal behaviour was then examined vis-à-vis the hydration curves.

2 Reconditioned waste

The initial characterization of the salt revealed that it was highly waterlogged at a water content of 60 wt. % after drying at 100°C. To improve the reproducibility of the tests, the salt was air-dried, after which the residual water content was approximately 16 wt. %. Detailed characterization of the air-dried salt revealed that it consisted of different hydration states of sodium carbonate (Na_2CO_3), with thermonatrite ($Na_2CO_3.H_2O$) being the most dominant. Additionally, trona ($Na_2CO_3.NaHCO_3.2H_2O$) occurred, in addition to small quantities of natron ($Na_2CO_3.10H_2O$) and gaylussite ($Na_2Ca(CO_3)_2.5H_2O$).

As initial experiments revealed that direct immobilization of the salt was ineffective due to the strongly hygroscopic nature of sodium carbonate, a pretreatment was necessary. As sodium carbonate is highly soluble, a double displacement reaction to form insoluble calcite ($CaCO_3$) was proposed as an effective way to improve compatibility with cementitious and alkali-activated matrices. A number of possible reagents exist, such as $CaCl_2$, $Ca(NO_3)_2$ and $Ca(OH)_2$. The former two were found to be ineffective as they either introduced new complications to the waste form (chloride attack in the case of $CaCl_2$) or negatively impacted the properties of the waste form (in the case of $Ca(NO_3)_2$). Therefore, $Ca(OH)_2$ was chosen as the reagent, with the additional benefit that the reaction (shown below) produces NaOH, which acts as an activator for the precursor of the alkali-activated matrices.

$$Na_2CO_3 + Ca(OH)_2 \rightarrow CaCO_3 + 2NaOH$$

Pretreatment tests revealed that in addition to calcite, gaylussite was also formed as a reaction product. Gaylussite is a double carbonate intermediary between sodium and calcium carbonate end members. Thermodynamic modelling indicated that it is not a stable product in the long term, indicating that it is a metastable intermediary that reacts further to calcite in time.

After the pretreatment, the resulting sludge was incorporated into an alkali-activated or blended cementitious matrix. Waste loading, expressed as the weight percentage of air-dried salt residue relative to the total mass of the waste form, varied from 10 to 20 wt. % in the case of the alkali-activated matrices and 10 to 14 wt.% for the cementitious matrix. The fresh waste forms were cured under humid conditions (100% RH, room temperature) for 28 days to ensure that the waste form could withstand high humidity.

Table 2-1: Details of the recipes used for the immobilization of the molten salt residue. Abbreviations are as follows: BFS = blast furnace slag; MK = metakaolin; LF = limestone filler; L = limestone; LS = limestone sand; SF = silica fume; AAM = alkali-activated material.

Recipe	Water/binder ratio	Waste loading, %
AAM_MK: Precursor: MK, Activator: K_2SiO_3 (CVRez)	0.33	10
	0.37	15
	0.43	20
AAM_BFS**:** Precursor: BFS, Activator: NaOH, sodium disilicate (SCK CEN)	0.54	10
	0.56	20
Blended cement: CEM I, BFS, SF, LF, LS (SCK CEN)	0.90	14
	0.78	10

Additional experiments were carried out using a metakaolin-based geopolymer recipe developed by CVRez. Their recipe was based on the commercial geopolymer mix Baucis LK, which is available

from České Lupkové závody a.s. Baucis. Baucis LK consists of metakaolin Mefisto L05 and an alkaline activator consisting of 35 wt. % potassium silicate. The chemical and physical properties of the Mefisto L05 MK, as declared by the manufacturer, are shown in Table 2-2.

Table 2-2: The chemical composition Mefisto L05, used in Baucis LK geopolymer.

Mefisto L05		
Oxides	**Typical content (wt. %)**	**Guaranteed content (wt. %)**
Al_2O_3	40.10	min. 38.0
SiO_2	54.10	max. 57.0
K_2O	0.80	max. 0.9
Fe_2O_3	1.10	max. 1.80
TiO_2	1.80	max. 2.00
MgO	0.18	max. 0.4
CaO	0.13	max. 0.2

The experiments were aimed at MSO waste immobilization in a MK-based matrix. The waste salt was produced from a different batch than that used by SCK, but its mineralogical and chemical compositions were similar. They were air-dried and crushed to a particle size of 0.1 mm. After this treatment, the waste had an average moisture content of 45 wt. %. The waste loadings of 10, 15, and 20 wt. % were tested for the calorimetric measurements. Although the waste loading was similar to that tested on the SCK waste forms, the salt content was lower because of the higher moisture content.

An improved recipe from the Baucis LK manufacturer was used for the upscaling experiments. The recipe was named LK10, based on the MK-based geopolymer Baucis LK with an additional 10 wt. % geopolymer added as filler. Table 2-3 shows the compositions of the materials used.

Table 2-3: The used recipe for the Scale-up experiments.

Total weight (kg)	Waste loading 15 wt. % (kg)	Metakaolin (kg)	Metakaolin filler (kg)	Activator (kg)
200	30	83.33	20	66.67

3 Heat transfer model

To predict the thermal evolution in the waste drum, the following energy balance equation can be used:

$$C_{p,eff}\rho_b \frac{\partial T}{\partial t} = \nabla \cdot \lambda_{eff} \nabla \mathrm{T} + \dot{Q}_{OPC} + \dot{Q}_{BFS} + \dot{Q}_{SF} + \dot{Q}_{waste} \quad (1)$$

where T is the temperature, $C_{p,eff}$ is the effective specific heat capacity of the hardened waste form (J/kg/K), ρ_b is the effective bulk density of the hardened waste form (kg/m^3), λ_{eff} is the effective thermal conductivity of the hardened waste form (W/m/K), and $\dot{Q}_{OPC}$, $\dot{Q}_{BFS}$, $\dot{Q}_{SF}$ and $\dot{Q}_{waste}$ are the heat production rates of OPC, BFS, SF, and liquid waste, respectively.

However, it is tedious to determine the heat release rates of individual recipes within a composite mix and will involve many experiments for each recipe, let alone many promising recipes. As the goal of this exercise is to mainly estimate the maximum temperature at the drum scale, one may replace the individual $\dot{Q}_i$ with one composite heat production rate, $\dot{Q}_c$. With this, Equation (1) can be rewritten as:

$$C_{p,eff}\rho_b \frac{\partial T}{\partial t} = \nabla \cdot \lambda_{eff} \nabla \mathrm{T} + \dot{Q}_c \quad (2)$$

$$\dot{Q}_c = \dot{\alpha} Q_{inf} c \quad (3)$$

where α is the degree of hydration (unitless), as defined in Equation (4) [3]; Q_{inf} is the maximum heat of hydration of the binders (J/kg); and c is the weight of the binder per m^3 (kg/m^3) of the waste form.

$$\alpha = e^{\left[-\left(\frac{\tau}{t_e}\right)^{\beta}\right]} \quad (4)$$

where τ is the characteristic time and β is an empirical parameter. All of these were calibrated based on the cumulative heat release curve for a given recipe obtained from isothermal calorimetry using Equation (3). t_e is the equivalent time, which differs from the actual time t in Equation (2). It is defined via [4]:

$$t_e = \int_0^t e^{\frac{-E_a}{RT}\left[\frac{1}{T_{iso}} - \frac{1}{T}\right]} dt \quad (5)$$

where E_a is the activation energy of the waste form, R is the universal gas constant, T_{iso} is the temperature at which the isothermal calorimeter was maintained. The concept of equivalent time is an important concept that ensures that Equation (3) can be used at any other arbitrary temperature T.

The standard approach to determine E_a is by carrying out isothermal calorimetric experiments for a given recipe at least at four different temperatures, as demonstrated in [26]. However, this again is a resource-intensive undertaking.

$C_{p,eff}$ is derived from the semi-adiabatic calorimeter measurements as follows:

$$C_{p,eff} = \frac{\Delta Q_{pb} m_b - (\Delta Q_e + \Delta Q_c)}{m_s \Delta T} \quad (6)$$

$$\Delta Q_e = \alpha_c \Delta T$$

$$\Delta Q_c = C_{pc} \Delta T$$

where Q_{pb} is the heat produced by the hydration reaction per unit weight of the binder (J/kg binder), m_b is the mass of the binder (in this case, 1 kg), Q_e is the heat released to the environment, Q_c is the heat absorbed by the calorimeter, m_s is the mass of the sample (waste form) in the calorimeter (kg), α_c is the heat transfer coefficient of the calorimeter provided by the manufacturer (J/K), and C_{pc} is the specific heat capacity of the calorimeter casing provided by the manufacturer (J/K). The Δ indicates the change sampled every 1 h. The data collected from the calorimeter typically lasts 7 days. Thus, the $C_{p,eff}$ is the average of the entire duration to avoid an oscillatory output.

As such, no specific experiments have been carried out to determine λ_{eff}. However, given that the hardened waste form has high water content, it is reasonable to assume that its value is less than one.

The calculation strategy based on the above formulation is shown in Figure 3-1. In principle, this involves an isothermal calorimetric heat release curve at a reference temperature, a semi-adiabatic calorimeter temperature evolution curve, and heat loss data that form the fundamental input to the model.

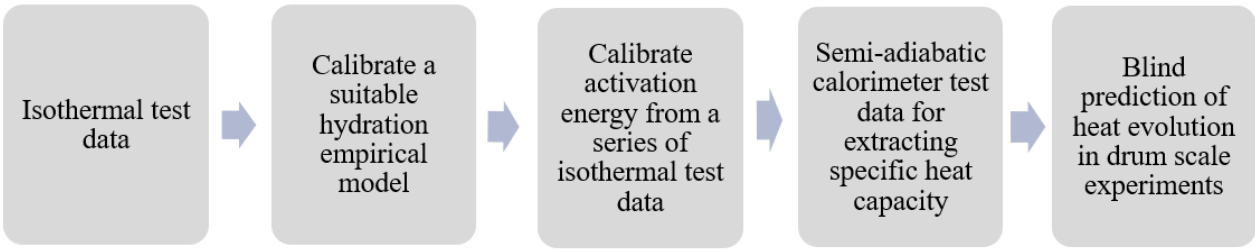

Figure 3-1: Calculation strategy to predict temperature evolution at the drum scale.

In conclusion, the following material parameters are required to solve the energy balance equation (Table 3-1).

Table 3-1: Material parameters of the waste form for calculating temperature evolution at the drum scale.

	Description	Notation	Units
1	Effective Specific heat capacity	$C_{p,eff}$	J/Kg/K
2	Effective bulk density	ρ_b	$\mathrm{kg/m^3}$
3	Effective thermal conductivity	λ_{eff}	W/m/K
4	Maximum heat of hydration of the binder (not of waste form)	Q_{inf}	J/kg
5	Binder density	c	$\mathrm{kg/m^3}$
6	Characteristic time of the heat release rate curve	τ	d
7	Empirical parameter of the degree of hydration equation (Equation (4))	β	-
8	Activation energy (Equation (5))	E_a	$\mathrm{kJ/mol}$
9	Reference temperature of the isothermal calorimetric experiment (unless otherwise stated = 293.15 K)	T_{iso}	K

4 Experiments

4.1 Calorimetric experiments

4.1.1 Isothermal calorimetry

Isothermal calorimetric experiments were carried out to determine the heat of hydration/geopolymerization for various recipes. An I-Cal 8000 HPC (Calmetrix, Inc.) isothermal calorimeter, which is a High Precision Calorimeter with 8 channels that can be used to test cement paste, mortar, and concrete, was used. The equipment consists of a temperature-controlled chamber with 8 independent channels. Two samples per test case were analyzed (approximately 100 g of each sample). The heat released by the samples was measured during the first 7 days of hydration at various temperatures.

Prior to mixing samples, the constituting components were heated at a slightly elevated temperature relative to the temperature of the calorimeter (e.g., components were heated at 55 °C when the calorimeter was at 50 °C). The components were removed from the oven, mixed, and transferred into the calorimeter as quickly as possible. This procedure aims to minimize the cooling of the sample prior to insertion into the calorimeter so that no energy is required to heat the sample inside the calorimeter before measuring the exothermic response related to dissolution and other processes. Inevitably, all samples at elevated temperatures, i.e., 35 °C and 50 °C, displayed some amount of cooling, evident as a negative initial heat flow in the output of the calorimeter. This artifact is corrected mathematically by monitoring the inflection point at which the heat flow has reached its minimum, which is assumed to be the point at which the sample itself starts to contribute heat to the calorimeter instead of just absorbing it to reach the correct temperature.

Figure 4-1: I-Cal 8000 HPC isothermal calorimeter.

4.1.2 Semi-adiabatic calorimetry

The heat of hydration was determined using semi-adiabatic calorimetry [11]. The measurement uses a semi-adiabatic calorimeter (Langavant Controlab-Perrier, France) with a reference calorimeter (with an inert sample hydrated for more than 1 year) and three calibrated measured calorimeters. This measurement provides the temperature reached by the sample as a function of time. It also gives the 'warm' of the sample, which is the temperature increase in comparison with the reference

sample. The heat of hydration is given as joule per gram (J/g) of the binder. Semi-adiabatic measurements were performed by pouring approximately 1 kg of the fresh mix into an aluminum container with a thermocouple inside. The temperature change and heat of hydration were analyzed over seven days, and the data were analyzed using CemTech software (Controlab, France).

Figure 4-2: Langavant semi-adiabatic calorimeter.

4.2 Drum scale experiments

In the scope of D6.7, CV Rez conducted scale-up experiments involving conditioning an MSO waste into the metakaolin base matrix. For this purpose, CV Rez used a solidification device capable of scale-up operations, the dimensions of which are shown in Figure 4-3. Firstly, a top mixer affixed to a movable shoulder facilitated both horizontal and vertical movements within the drum. The mixer offers rotational options in both the right and left directions and operates at a maximum speed of 3000 rpm. The operating speed is based on a combination of the viscosity and operator experience. To complement this, the device features a drum rotator that rotates independently of the mixer.

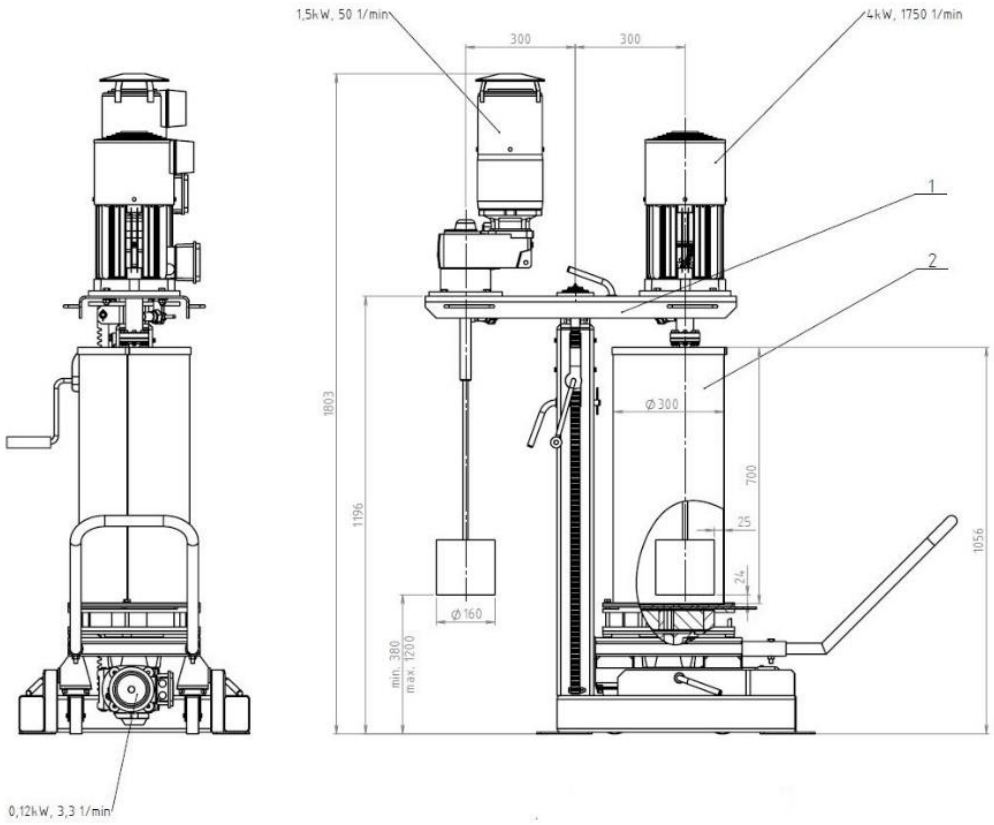

Figure 4-3: CVRez scale-up solidification technology.

For the scale-up experiments, a 100 L drum was selected. Due to the time management and lack of stock of drums, two types of drums were used. The data for each drum are presented in Table 4-1

Table 4-1: The properties of used drums.

Black 100 L drum		Blue 100 L drum	
Height (mm)	820	Height (mm)	706
Diameter (mm)	482	Diameter (mm)	450
Total volume (L)	120	Total volume (L)	115
Sheet thickness (mm)	0.7	Sheet thickness (mm)	0.6

A specially designed lid featuring six entry points for the thermocouples is shown in Figure 4-4. Each thermocouple is equipped with three temperature sensors (bottom, middle and top) situated at distances of 25, 325 and 675 mm from the base of the drum post-insertion. Surface thermocouples with one temperature sensor were positioned at distances of 100, 200, 300, 400, 500 and 600 mm from the drum base. The layout of these temperature sensors was based on thermal simulations carried out by SCK CEN to obtain the most optimum information from the experiments.

Figure 4-4: The temperature measurement setting in 100 L black drum (left), 100 L blue drum (middle) and thermocouple position in the drum lid (right).

Mixing of the MK and alkali activator occurred in stages. After the previous tests, it was determined that the alkali activator had to be added first, followed by MK and waste, to improve workability and increase homogeneity. Overall, the mixing took three stages, and each stage took 10 min to achieve proper mixing. Table 4-2 shows the materials added at each stage for each experiment. After mixing, the drum was closed with a lid, and thermocouples were inserted into the tubes and attached to the outside surface of the drum. The temperature was measured until the temperature inside the drum decreased to the laboratory temperature.

Table 4-2: The material added in each stage of the experiment.

Stage / Material	1	2	3
Activator (kg)	25	25	16.67
Metakaolin (kg)	40	40	23.33
Waste (kg)	12	12	6

5 Drum scale model set-up

The 2D-axisymmetric simplification of the 100 L drum is shown in Figure 5-1.

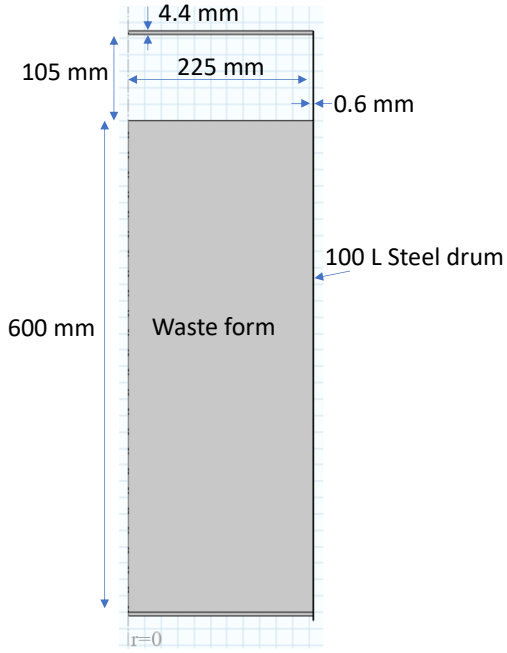

Figure 5-1: Geometry of the drum.

Initially, both the waste form and the drum are assumed to be at 295.15 K, based on in situ temperature sensors. Convective heat losses are allowed to occur on all sides, except across the symmetry plane, using the heat transfer coefficient h_c. For all cases, radiative heat loss is allowed from the exposed surface (see Figure 5-1) of the waste form by assuming high emissivity. Note that the theory of surface-to-surface radiation is not covered in Section 3, as this is beyond the scope of this report. However, for completeness, the reader is referred to page 252 of the COMSOL user manual [16]. The hydration and thermal parameters are dealt with separately in Section 5. Additional parameters required for model execution are listed in Table 5-1.

Table 5-1: Material parameters required for the drum scale simulations.

	Parameter	Units	All scenarios
1	h_c (top and sides)	W/m^2/K	10
2	h_c (bottom)	W/m^2/K	2
3	λ_{eff} (steel)	W/m/K	16
4	ρ_b (steel)	$\mathrm{kg/m^3}$	8000
5	ϵ (steel)	-	0.23
6	ϵ (waste surface)	-	0.94

6 Results

6.1 Calorimetric experiments

6.1.1 Recipe: AAM with metakaolin (CVRez)

Figure 6-1 shows the cumulative hydration curves for 10%, 15%, and 20% waste loading at temperatures 20 °C and 50 °C. The expected heat output of a metakaolin geopolymer is similar to that of an alkali-activated slag: an initial exothermic peak related to the wetting and dissolution of the precursor, followed by a (smaller) broad exothermic peak related to the formation of N-A-S-H gel.

At 20°C, for the lowest waste loading, there are three peaks observable. The first is related to the initial dissolution, and the other two are related to gel formation. The presence of two separate gel formation events may be related to the nature of the precursor. Commercial Mefisto metakaolin is rich in iron (1.1% Fe_2O_3), which is unusual for metakaolin. It is possible that instead of pure metakaolin, this precursor consists of a mix of metakaolin and slag, which would explain the existence of these separate peaks. At higher waste loadings, the separate peaks are not observable, possibly due to the lower amount of precursor available. As with the alkali-activated slags, there was a delay in the start of gel formation, with the initial gel formation starting after 8 hours for the lowest waste loading and after 27 hours for the highest waste loading.

At elevated temperatures, the heat output increases with increasing temperature. Again, no secondary peaks were observed, indicating that the same mechanisms were active in the alkali-activated slags.

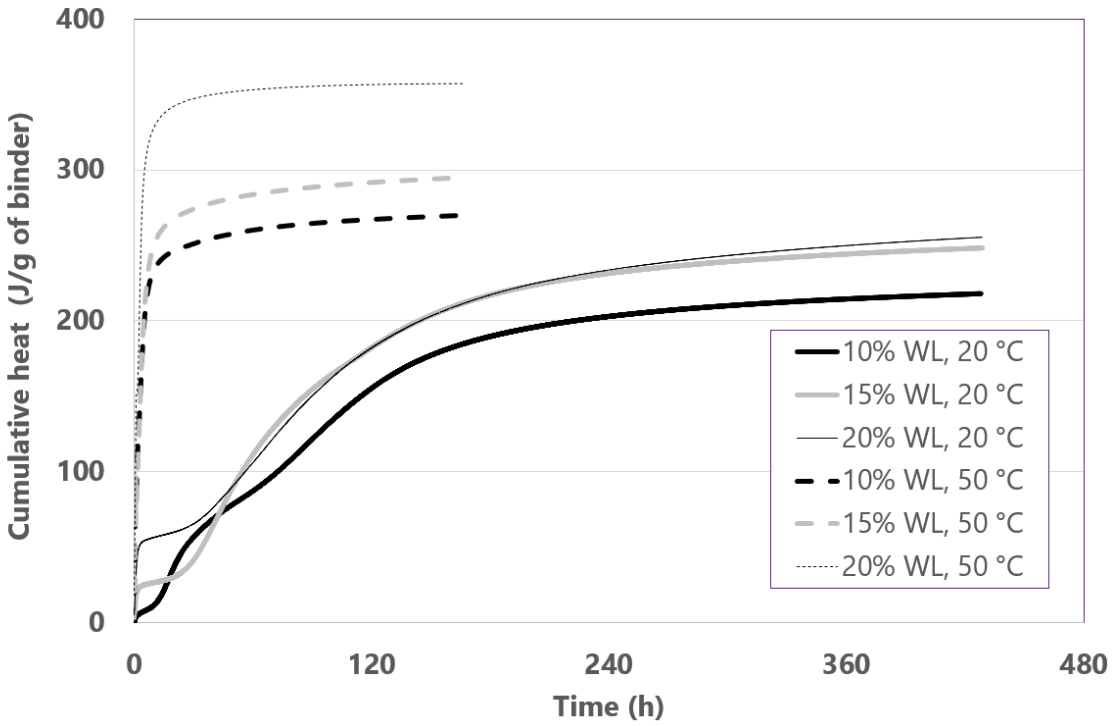

Figure 6-1: Measured cumulative heat for the AAM with metakaolin binder (CVRez) at various loadings and temperatures.

6.1.2 Recipe: AAM with BFS (SCK CEN)

Figure 6-2 shows the cumulative hydration curves for 10% and 20% waste loading at temperatures 20 °C, 35 °C and 50 °C. The thermal output of an alkali-activated BFS was characterized by two phases. Initially, a strong exothermic peak related to wetting and dissolution of the slag precursor was observed. After this initial heat pulse, a (short) dormant period, which can be interpreted as an induction period similar to that observed in cement hydration; dissolution products build up in concentration until a threshold is reached to allow the formation of the C-(N-)A-S-H gel, which constitutes the matrix of alkali-activated slags.

At 20 °C, both phases can both be observed. In both cases, the peak intensities of the dissolution and gel-building peaks were lower in the 20 wt. % waste loading sample, which is unsurprising given the lower amount of precursor available to dissolve and react. This is also reflected in the cumulative heat output. The dormancy period between the two waste loadings was markedly different; in the 10 wt. % waste loading sample, there is a significant overlap between the two peaks, indicating that gel formation happened almost concurrently with precursor dissolution. Meanwhile, there was a delay of approximately 8 hours after mixing before gel formation started in the 20% waste-loading sample. Again, the smaller amount of precursor is likely to be a contributing factor, as it would take longer for the necessary amount of solutes to be available to initiate gel formation.

The cumulative heat release of these samples at elevated temperatures increases as the temperature increases, which is expected because an increase in temperature promotes the dissolution of the precursor and thus furthers the reaction degree. Remarkably, no secondary peaks were observed for either waste loading at these temperatures. As the cumulative heat continued to increase (slowly) after the initial peak, two phenomena were likely to occur. On the one hand, gel formation occurs concurrently with the dissolution of the precursor, which occurs faster owing to the elevated temperature. However, after the initial dissolution peak, dissolution and gel formation continued slowly over time.

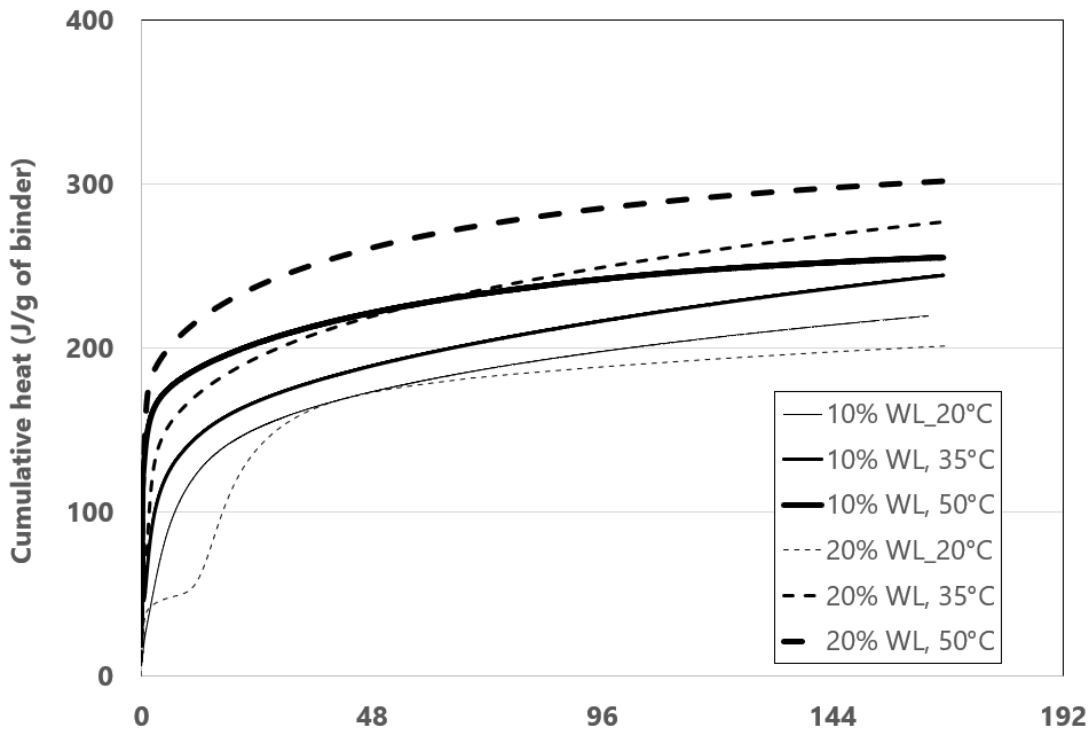

Figure 6-2: Measured cumulative heat for the AAM with BFS binder (SCK CEN) at various waste loadings and temperatures.

6.1.3 Recipe: Blended cement (SCK CEN)

Isothermal calorimetry was used to measure the heat of hydration of the two mixes using blended cement: one sample with a waste loading of 10% and a w/b ratio of 0.78, and one sample with a waste loading of 14% and a w/b ratio of 0.90. The cumulative heat curves for the two recipes tested with the blended cement samples are shown in Figure 6-3.

The total heat produced by the 14% WL sample was higher than that of the 10% WL sample. This was mainly due to the higher initial heat in the first 6 hours of hydration. For the 14% WL sample, there was little, or no induction period compared to the 10% WL sample. Two factors can explain this behaviour: the w/b ratio and waste composition.

The predominant factor for this behavior is the high amounts of $CaCO_3$ and NaOH present in the waste. A higher waste loading yielded higher $CaCO_3$ and NaOH in the mix. The presence of NaOH shortened the induction period and increased the heat produced at an early age in the mortars. The presence of $CaCO_3$ has also been reported to accelerate the hydration of cement by the filler effect.

The w/b ratio can also affect the hydration heat. A lower w/b ratio can increase the heat generated at a very early age. In the mix studied in this work, the very low amount of OPC and the presence of SCM mitigated this behaviour. However, after this initial period, a lower w/b ratio results in a lower heat of hydration. It can be observed in the curves that the heat of the WL 14% sample, with a higher w/b ratio, gives a higher heat over time when compared to the WL 10% sample.

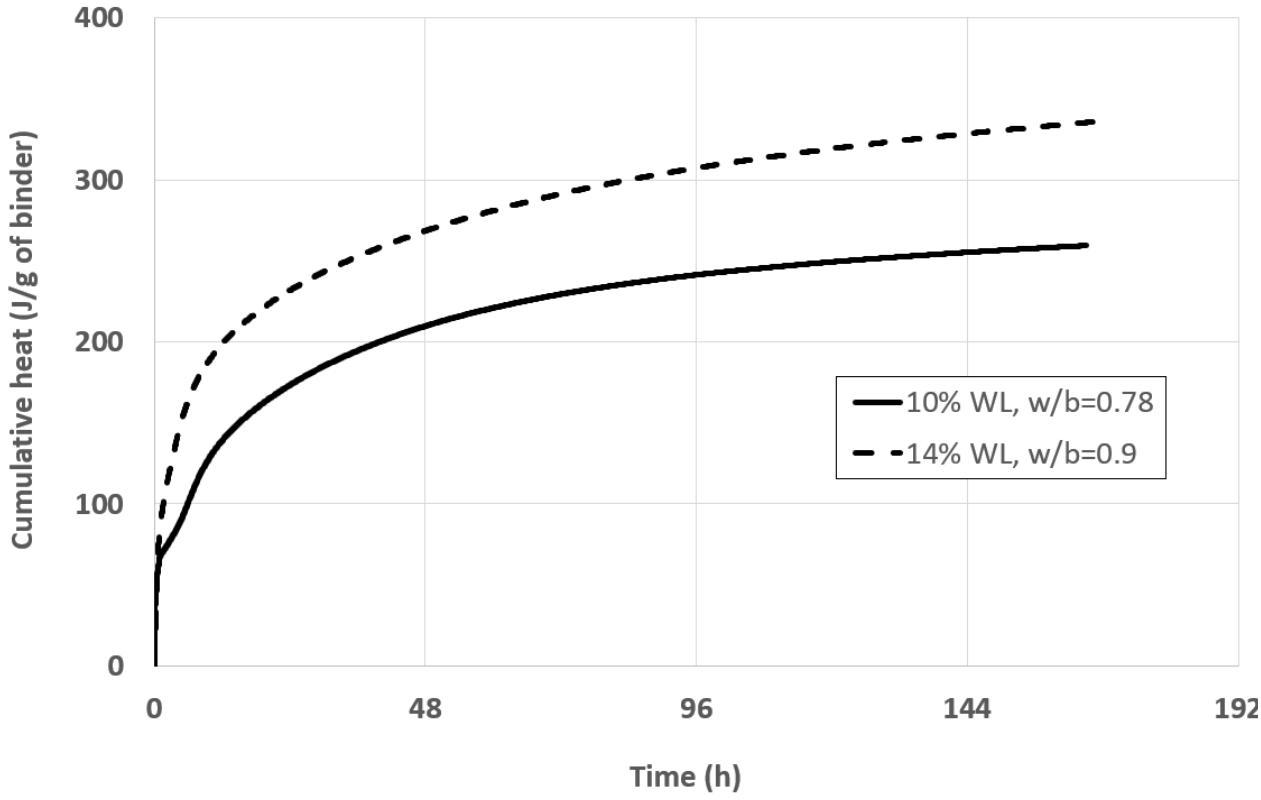

Figure 6-3: Measured cumulative heat for the blended cement (SCK CEN) at various waste loadings.

6.1.4 Calibration of hydration model parameters

The hydration model (Equation (4)) was calibrated against the cumulative heat release (hydration) curves obtained from the isothermal calorimetric tests, as shown in Figure 6-4. As Equation (4) was originally proposed for ordinary Portland cement material, it may not be able to accurately capture the hydration curves of composite materials such as the AAM and blended cements used in this study. However, the main objective of this study was to obtain the maximum temperature for a given recipe. With this objective, the calibration results are more than satisfactory, as shown in Figure 6-4.

Activation energy, Ea (Equation (5)), for the different recipes was determined based on the hydration curves obtained at different temperatures using the modified ASTM method [5]. As for the thermal conductivity, no experimental data were available. However, given that all the recipes had a higher water content, it was assumed that the thermal conductivity was < 1 W/m/K. A crude sensitivity analysis with respect to the drum scale temperature data for the AAM_MK with 15% waste loading yielded 0.86 W/m/K as the best fit. This value was applied to all recipes. Thus, there is a large uncertainty in this parameter.

The semi-adiabatic calorimeter results were available only for the AAM_MK, which had 15% waste loading. Thus, the specific heat capacity was determined for this recipe using Equation (6). However, given that the waste loadings for all other recipes do not significantly differ and acknowledging that the oxide compositions of the different precursors are different, it is assumed that the specific heat capacity determined for AAM_MK 15% waste loading is equally valid for these. This also implies that there is large uncertainty in this parameter.

Table 6-1: Hydration/thermal material parameters of the waste form obtained from lab experiments.

	Parameter	Units	AAM_MK			AAM_BFS		Blended cement	
			10% WL	15% WL	20% WL	10% WL	20% WL	10% WL	14% WL
1	$C_{p,eff}$	J/Kg/K	1952	1952	1952	1952	1952	1952	1952
2	ρ_b	kg/m³	1940	1930	1920	1920	1940	1824	1917
3	λ_{eff}	W/m/K	0.86*	0.86*	0.86*	0.86*	0.86*	0.86*	0.86*
4	Q_{inf}	J/g	276	298.3	388	333	390	360	565
5	c	kg/m³	1304.5	1229	1154	875	769	640	625
6	τ	h	59	55	69.4	11.6	336	8.7	14.6
7	β	-	0.79	0.9	0.51	0.31	0.29	0.37	0.26
8	E_a	kJ/mol	63	63	63	43	76	63	63
9	T_{iso}	K	293.15	293.15	293.15	293.15	293.15	293.15	293.15

** Assumed because the water content of the system is high.*

AAM_MK (CVRez)

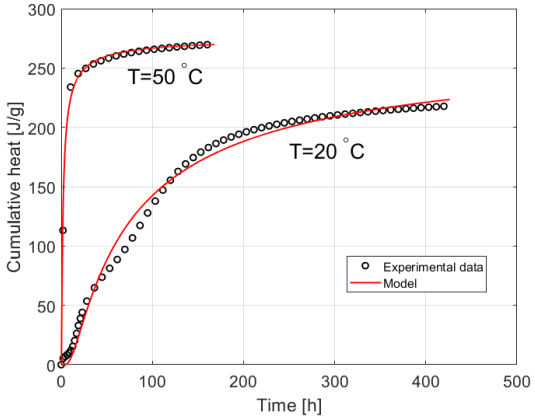

10% waste loading

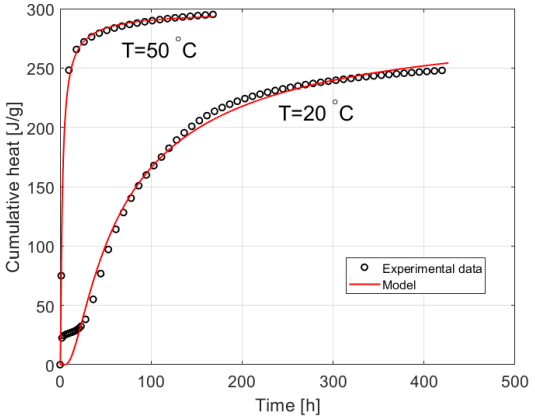

15% waste loading

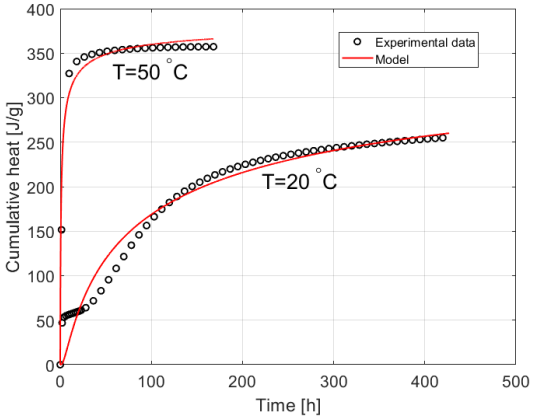

20% waste loading

AAM_BFS (SCK CEN)

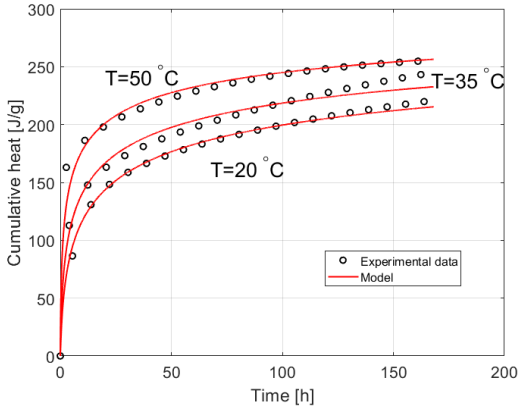

10% waste loading

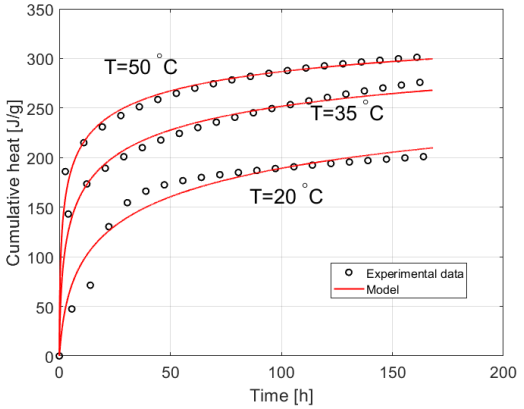

20% waste loading

Blended cement (SCK CEN)

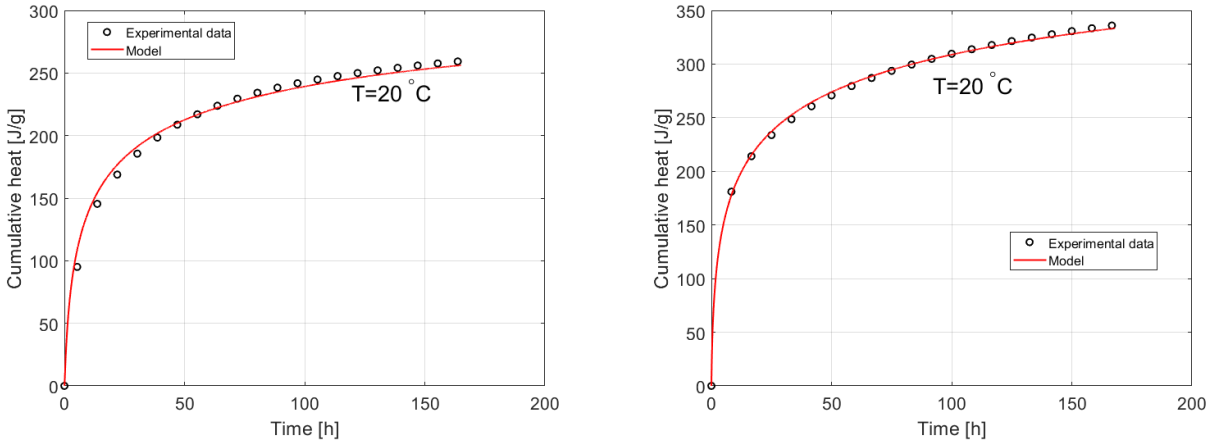

10% waste loading

14% waste loading

Figure 6-4: Calibrated results of hydration data for various recipes, temperatures and waste loadings.

6.2 Drum scale thermal simulations

As stated earlier, CVRez carried out drum-scale experiments for only one formulation, i.e., AAM with metakaolin precursor (AAM_MK). Figure 6-6 shows a comparison of measured vs. simulated temperature at three locations in the drum as shown in Figure 6-5. From a phenomenological perspective, AAS_MK produced significant heat during the first day of hydration and geopolymerization, followed by a rapid drop in heat production during the next few days. The peak temperature at the core of the drum reached approximately 90 °C. Note that this is only for a 100 L drum. However, the size of the waste drums is typically greater than 200 L. Therefore, the AAS_MK recipe is likely to yield peak temperatures in excess of 100 °C under realistic conditions. Such high temperatures are not acceptable for traditional cement binders because of potential pathologies such as thermal cracking and delayed ettringite formation. However, such pathologies were not immediately observed in the current study, at least during the short-term experimental period. Thus, long-term studies are required to confirm the stability of the matrix at higher temperatures.

The model results matched reasonably well with the peak-measured temperature data at the core. The predictions at the bottom and sides were not well captured. This is to be expected because the values of thermal conductivity and heat transfer coefficient were assumed, which can have a larger impact on the results compared to the core of the drum, where the conditions are close to the adiabatic state. Note that the main objective of this simulation work was to predict the peak temperature under realistic conditions and not to capture the detailed thermal response for which an extensive experimental programme is required to identify all the material parameters and their uncertainties.

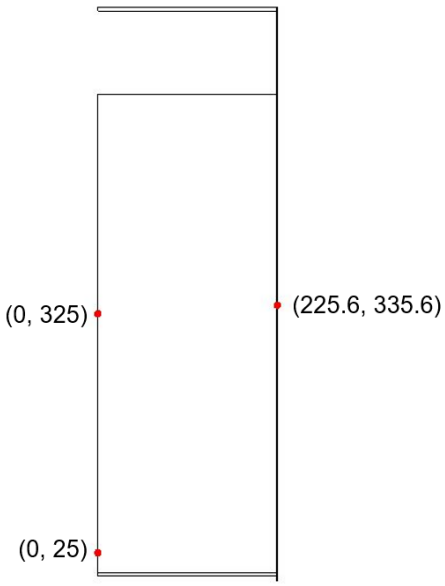

Figure 6-5: Location of temperature sensors for comparison with simulated data (dimensions in mm).

Figure 6-7 shows the blind predictions for the CVRez samples with waste loadings of 10% and 20%. Although the cumulative heat produced by 20% waste loading (388 J/g) was much higher than that produced by 15% waste loading (298.3 J/g), the peak temperature for 20% waste loading was marginally lower than that for 15% loading. This is because the binder density for 20% waste loading (1154 kg/m^3) is smaller than that for 15% waste loading (1229 kg/m^3), thus reducing the effective heat release for the former. However, because the heat release rate for the 20% waste loading was higher, the time of the peak temperature was advanced (≈ 19 h) compared with the other waste loadings (≈ 25 h). For 10% waste loading, a lower peak temperature was predicted with a slight delay in the time of the peak.

The hydration rate of the remaining recipes (Figure 6-4) was much higher than that of the AAM_MK recipes. Accordingly, the model predicts a rapid rise in temperature, with the peak temperature reaching approximately 10 h, as shown in Figure 6-7. The model shows that the temperature evolution is not sensitive to different waste loadings in the case of AAM_BFS. However, with blended cements, the effect of waste loading is rather sensitive. The difference in the peak temperature between 14% and 10% waste loading was approximately 16 °C. This was because of the higher heat release in the case of 14% waste loading. This is slightly higher than the difference found for AAM_MK, which is approximately 10 °C. In conclusion, given that the thermal parameters such as specific heat capacity, thermal conductivity, and activation energy are identical or similar for all cases, the predicted thermal behaviour can be easily explained by the hydration curves (Figure 6-4) and the associated parameters in Table 6-1.

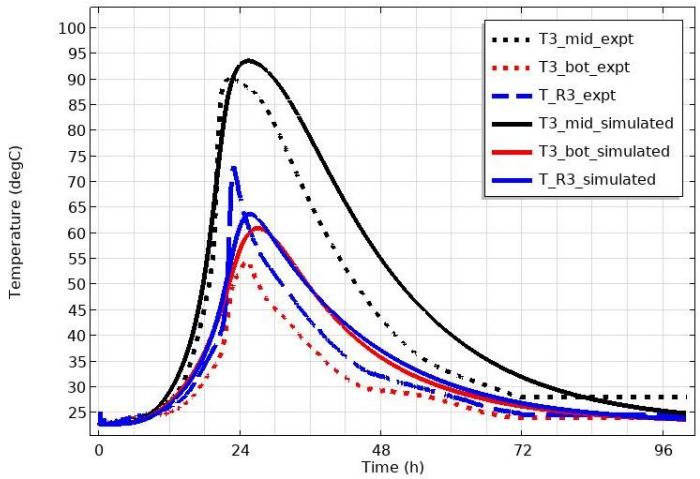

Figure 6-6: Maximum temperature evolution in the drum filled with CVrez recipe with a waste loading of 15%.

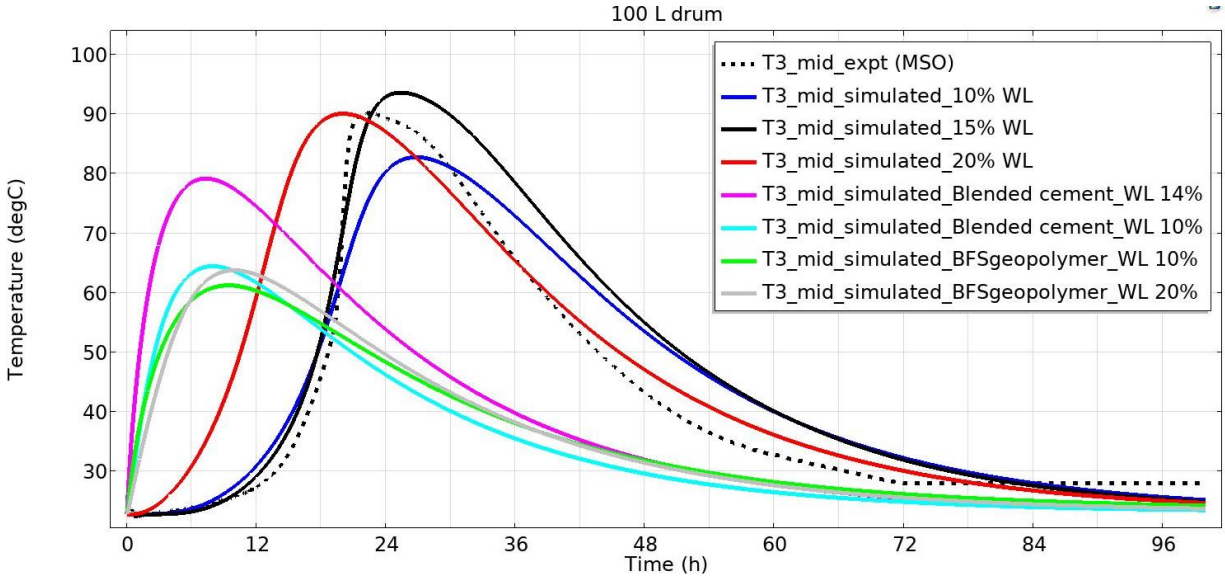

Figure 6-7: Maximum temperature evolution in the drum filled with different recipes listed in Table 2-1.

7 Summary and challenges

This report presents an experimental-numerical study of the thermal evolution of reconditioned MSO residue waste emplaced in 100 L drums. Three binders, AAM_MK, AAM, BFS and blended cement mix, were used for this purpose with carefully designed waste loadings. The study mainly considered isothermal calorimetry experiments of all the above recipes at SCK CEN to develop a comprehensive dataset of hydration curves that formed a direct input to the source term of a heat transfer model. Drum-scale experiments on reconditioned MSO residue waste were successfully designed and executed by CVRez. Appropriately designed thermal sensors in the 100 L drums captured the temperature evolution at various locations. A standard heat transfer model was used for blind predictions of the thermal evolution in the drum. As the drum-scale experiments were conducted only with AAM_MK binder, the drum scale thermal evolution for the remaining recipes was purely a theoretical estimate based on the numerical model.

7.1 Contributions

Key contributions to the PREDIS project are summarized below:

a) The calorimetric measurements of the different waste forms showed that the addition of molten salt residue delayed the hydration/geopolymerization in both cementitious and alkali-activated matrices. This effect is primarily related to the decrease in precursor/clinker in the matrix, which reduces the amount of solutes necessary for gel formation and thus lengthens the dormancy period. Increasing the temperature of the mixture to 35 or 50°C had the opposite effect, effectively eliminating the dormancy period and starting gel formation concurrently with the dissolution of the precursor due to enhanced dissolution of precursor/clinker at higher temperatures.
b) The scale-up tests primarily provided valuable insights into the behaviour and performance of alkali-activated materials in large-scale drums.
c) In general, the numerical model was able to capture the main features of the thermal evolution, particularly the peak measured temperature data at the core. The predictions at the bottom and sides were not well captured because of the lack of availability of material properties for the heat-transfer model.
d) The model also showed that the AAM_MK recipe reached maximum temperature at approximately 1 d and in excess of 90 °C. Given that typical drum sizes used by waste producers are in excess of 200 L, the use of this recipe will yield maximum temperatures in excess of 100 °C after casting.
e) As no drum-scale experiments were available for the remaining recipes, the blind predictions show that the peak temperatures for these recipes can be much smaller and the time of peak being earlier, which is attributable to the higher rate of hydration/geopolymerization and lower binder density in these recipes compared to AAM_MK.
f) Given the success of simulating the temperature evolution at the drum scale using a standard heat transfer model with laboratory-based data, significant costs can be saved by minimizing the number of drum-scale experiments.

7.2 Challenges

Key challenges are summarized below:

a) Isothermal calorimetric measurements at different temperatures necessitate heating the components of each mix to the required temperature, followed by rapid mixing and transfer to the calorimeter to prevent cooling of the mixture. There is, however, an inevitable degree of cooling, which requires (imperfect) correction of the associated artifacts in the output. In the future, this can be improved by performing such experiments using a calorimeter that allows in-device mixing of samples, thereby eliminating the need to preheat and transfer samples to the calorimeter.

b) The order in which the components were added to the drum before and during the mixing process is important for achieving a homogeneous mixture. It is equally important to accurately monitor the temperature during curing of the sample. Maintaining a stable ambient temperature was also crucial for avoiding abrupt temperature fluctuations that could negatively affect the final sample. Alternatively, measuring ambient temperature will also suffice, as it helps to input correct boundary condition to the drum scale model.
c) As stated above, the model suggests that for AAM_MK type formulations, temperatures can significantly exceed 100 °C when used in realistic drum sizes. Therefore, for this type of material, the long-term effects of early exposure to high temperatures should be considered in future studies.

REFERENCES

[1] Galek et al. Conditioning of ashes of RSOW by geopolymer or cement-based encapsulation, PREDIS WP6 Report, https://predis-h2020.eu/publications-and-reports/ (accessed on 15th July 2024), 2023.

[2] Pedro Perez-Cortes, Inés Garcia-Lodeiro, Francisca Puertas, Maria Cruz Alonso, Effect of incorporating a molten salt waste from nuclear power plants on the properties of geopolymers and Portland cement wasteforms, Cement and Concrete Composites, Volume 142, ISSN 0958-9465, 2023.

[3] Schindler, A.K. and Folliard, K.J., Heat of Hydration Models for Cementitious Materials. ACI Materials Journal, 102, 24-33, 2005.

[4] Freiesleben Hansen, P. and Pedersen J., “Maturity Computer for Controlled Curing and Hardening of Concrete,” Nordisk Betong, 1, pp. 19-34, 1977.

[5] J.L. Poole, K.A. Riding, K.J. Folliard, M.C. Juenger, A.K. Schindler, Methods for calculating activation energy for Portland cement, ACI Mater. J., 104 (1), pp. 303-311, 2007.